

# Toward Certifying Maps for Safe Localization Under Adversarial Corruption

Johann Laconte<sup>1</sup>, Daniil Liusu<sup>1</sup> and Timothy D. Barfoot<sup>1</sup>

**Abstract**—In this paper, we propose a way to model the resilience of the Iterative Closest Point (ICP) algorithm in the presence of corrupted measurements. In the context of autonomous vehicles, certifying the safety of the localization process poses a significant challenge. As robots evolve in a complex world, various types of noise can impact the measurements. Conventionally, this noise has been assumed to be distributed according to a zero-mean Gaussian distribution. However, this assumption does not hold in numerous scenarios, including adverse weather conditions, occlusions caused by dynamic obstacles, or long-term changes in the map. In these cases, the measurements are instead affected by a large, deterministic fault. This paper introduces a closed-form formula approximating the highest pose error caused by corrupted measurements using the ICP algorithm. Using this formula, we develop a metric to certify and pinpoint specific regions within the environment where the robot is more vulnerable to localization failures in the presence of faults in the measurements.

## I. INTRODUCTION

Reliable localization is a vital task for self-driving robots, as it plays a key role in ensuring their safety and effective operation. However, sensors are susceptible to making errors, necessitating the implementation of robust safeguards to mitigate potential risks. In this paper, we focus on the domain of range-based localization, a technique relying on range sensors such as lidar or radar. In addition to being inherently noisy, these sensors can also encounter large, deterministic errors that heavily deviate from the common Gaussian noise assumption, posing significant challenges to accurate localization.

Measurement corruptions can be caused by diverse sources. For example, an occlusion may cause a portion of the environment to be completely blocked from the sensor’s view, leading to missing or inaccurate range readings. Similarly, adverse weather conditions, such as heavy snowstorms or fog, can distort the sensor measurements in a nonrandom manner [1]. Consistent measurement errors can also arise from long-term changes in an outdated map, including the presence of new buildings or parked cars. These factors result in systematic and deterministic errors that are significantly different from the statistical properties of Gaussian noise.

The ICP algorithm is established as one of the most popular approaches for estimating a robot’s pose using range sensors [2]. Depending on the map against which ICP is trying to localize, a corruption of the pointcloud can be more or less impactful. Figure 1 depicts some examples



Fig. 1: In the context of pose estimation, specific environments entail higher risks compared to others. For instance, a large intersection (left) offers limited landmarks for localization, whereas a suburban area (right) presents numerous houses and landmarks. Consequently, occlusions or map alterations at the intersection may lead to a significantly larger pose estimation error compared to the suburban area.

from the self-driving application. In a large intersection, few structures are close enough to provide good constraints for ICP. As such, any faulty measurement on the structures would have a great impact on the localization output. On the contrary, smaller streets with lots of houses and other obstacles provide a much safer environment, as ICP can now rely on a variety of landmarks to localize. Even though ICP is frequently equipped with robust outlier rejection features, some faults can still be considered as inliers and impact the accuracy of the localization process. While not necessarily large enough to break the localization process, these inlier faults can degrade the localization accuracy to a degree that may easily result in a crash in autonomous driving scenarios

Our paper aims to quantify the map-dependent resilience of the ICP localization algorithm. Our contributions are 1) a closed-form formula of the worst possible error on the pose for a given amount of corrupted points; 2) a visualization of the worst corruption by applying the faults to the measured pointcloud; and 3) a quantification of the resilience of the ICP for a specific map against corrupted measurements. We provide a quantitative analysis of our framework, as well as the evaluation of both structured and unstructured environments, showing that our framework can pinpoint dangerous locations in the event of corrupted measurements.

## II. RELATED WORK

Extensive research has been conducted in the field of aerospace engineering to address safety considerations. In this context, the majority of safety analyses are bound to the estimation of position using Global Navigation Satellite

<sup>1</sup> University of Toronto Institute for Aerospace Studies (UTIAS), 4925 Dufferin St, Ontario, Canada. {johann.laconte, daniil.liusu}@robotics.utias.utoronto.ca, tim.barfoot@utoronto.ca

System (GNSS) measurements. The safety of this estimation is based on the Hazardously Misleading Information (HMI) metric, which looks at the probability that the position estimate is sufficiently erroneous to be considered hazardous, while no fault detectors have been triggered. The detectors can take on various forms, but two are most prevalent: residuals and solution-separation methods [3], [4]. The residuals-based methods look at the measurement residuals coming from the estimation algorithm [5], such as the innovation in a Kalman filter [6]. In the event such residuals are higher than a threshold, a fault in the measurements is likely and an alarm is triggered. On the other hand, solution-separation-based methods try to isolate and discard a potentially faulty measurement from all measurements received at a given time; this method quickly becomes computationally expensive as every combination of measurements needs to be tested [7]. Recently, Arana *et al.* [8] proposed to adapt these methods to robotics. They used the HMI framework to monitor the safety of a landmark-based localization pipeline. Their work was adapted to batch estimation by Hafez *et al.* [9]. Finally, Chen *et al.* [10] used this framework to propose a way to enhance the safety of maps by adding well-placed landmarks in the environment. All of these previous efforts aim at certifying that the system will be able to detect faults, which is fundamentally different from certifying the well-being of the system. Indeed, a very poor map can be classified as safe as long as it is easy for the system to detect that its estimated pose is not right. As such, we propose a novel method to directly monitor the reliability of the localization process, and not its capability to detect hazardous events.

In this context, the notion of *localizability* is the standard for range-based localization. Localizability is defined as the capability of the localization system to produce a good estimate of the robot’s pose. This information is paramount in under-constrained environments, such as tunnel-like surroundings [11], where the localization process is prone to yielding bad estimates. Nubert *et al.* [12] proposed a way to learn the localizability in underground environments. Ebadi *et al.* [13] developed a method to monitor the degeneracy of ICP throughout the localization process by looking at the condition of the measurement matrix after linearizing the system. Similarly, Zhang *et al.* [14] proposed to model the safety of the localization in an environment using Fisher information. Finally, Aldera *et al.* [15] proposed to train a classifier to automatically label odometry estimates as good or bad, showing that rejecting poor solutions leads to a better overall estimate. Carson *et al.* [16] used a similar idea to classify the integrity in visual localization, removing inaccurate estimates. However, the localizability analysis does not encompass the possibility of corrupted measurements that can arise in numerous situations, such as adverse weather or occlusion from other dynamic obstacles. Indeed, the analysis relies solely on the measured pointcloud, without taking into account the possibility that large errors can add malicious information. We propose a way to not only examine the safety of the system under nominal conditions, but also its performance in situations where certain measurements may

provide adversarial information to the robot.

Within the area of compromised data, different works were conducted to explicitly assess the resistance of algorithms to corruption by generating, altering, or removing some measurements. Kong *et al.* [17] designed a benchmark that directly takes into account the corruption of the data coming from diverse sources, such as the weather or sensor failures. This benchmark was used to extensively test the algorithms and their resilience to different types of noise. Xiang *et al.* [18] proposed a method to generate and perturb pointclouds that lead a classification network to mislabel the scanned object. Cao *et al.* [19] developed a method to craft 3D obstacles that were not detected by deep learning algorithms working with lidar data. Yi *et al.* [20] proposed novel metrics for the safety of robotics algorithms, such as the robustness of a bad prior and the absence of updates. Delecki *et al.* [21] designed a method to characterize failures of lidar-based perception systems in adverse weather conditions. Using physics-based disturbances and reinforcement learning, they were able to find high-likelihood failures with relatively small input disturbances. Finally, Yoshida *et al.* [22] directly attacked a pointcloud to force the ICP algorithm to move to a desired target position instead of the ground truth. Our work is similar in spirit to these methods, but we propose a closed-form algebraic method to analyze the resilience of the ICP algorithm through corruption of the measurements.

### III. PRELIMINARIES

First, we offer a brief illustration of the process to transform pointcloud alignment into an approximated linear problem. Next, we introduce the methodology for modeling corruption in conventional estimation problems. Using these formulations, we derive a closed-form formula representing the maximum possible error in a pose estimate.

#### A. ICP Formulation

We briefly show a linear simplification of ICP. For one iteration, the measurement model is written as

$$\mathbf{q}_i = \mathbf{R}(\mathbf{p}_i + \mathbf{w}_i) + \mathbf{t}, \quad (1)$$

where  $\mathbf{p}_i$  are the points in the sensor frame,  $\mathbf{q}_i$  are the points in the map frame, and  $\mathbf{w}_i \sim \mathcal{N}(\mathbf{0}, \sigma^2 \mathbf{I})$  is the noise on the measured point  $\mathbf{p}_i$ ,  $\mathbf{I}$  being the identity matrix. The matrix  $\mathbf{R}$  and vector  $\mathbf{t}$ , respectively, denote the rotation and translation components of the pose. Assuming the rotation  $\mathbf{R}$  between the scan and map pointclouds is small, we can use the small-angle approximation  $\mathbf{R} \approx \mathbf{I} + \phi^\wedge$  and linearize the relation as

$$\begin{aligned} \mathbf{q}_i &\approx (\mathbf{I} + \phi^\wedge)\mathbf{p}_i + \mathbf{R}\mathbf{w}_i + \mathbf{t} \\ &= \mathbf{p}_i - \mathbf{p}_i^\wedge \phi + \mathbf{R}\mathbf{w}_i + \mathbf{t} \\ &= [\mathbf{I} \quad -\mathbf{p}_i^\wedge] \begin{bmatrix} \mathbf{t} \\ \phi \end{bmatrix} + \mathbf{p}_i + \mathbf{w}'_i, \end{aligned} \quad (2)$$

where  $(\cdot)^\wedge$  is a cross-product operator transforming the vector to a  $3 \times 3$  skew-symmetric matrix [23].

In the case of point-to-plane ICP with unit normals  $\mathbf{n}_i$  in the map frame, we project the measurement points  $\mathbf{p}_i$  onto

the associated normals  $\mathbf{n}_i$ . Reworking (2) and stacking the  $N$  measurements into one vector  $\mathbf{y}$ , we have the linear system

$$\underbrace{\begin{bmatrix} \mathbf{n}_1^T(\mathbf{q}_1 - \mathbf{p}_1) \\ \vdots \\ \mathbf{n}_N^T(\mathbf{q}_N - \mathbf{p}_N) \end{bmatrix}}_{\mathbf{y}} = \underbrace{\begin{bmatrix} \mathbf{n}_1^T & -\mathbf{n}_1^T \mathbf{p}_1^\wedge \\ \vdots & \vdots \\ \mathbf{n}_N^T & -\mathbf{n}_N^T \mathbf{p}_N^\wedge \end{bmatrix}}_{\mathbf{A}} \underbrace{\begin{bmatrix} t \\ \phi \end{bmatrix}}_{\mathbf{x}} + \mathbf{w}, \quad (3)$$

with  $\mathbf{w} \sim \mathcal{N}(\mathbf{0}, \sigma^2 \mathbf{I})$ . This formulation has two main assumptions: known data association and a noniterative approach. While these assumptions may appear restrictive, we demonstrate in Subsection V-A that they actually establish a suitably conservative approximation of the error of the ICP algorithm.

### B. Problem Statement

In robotics, many problems can be formed as a least-squares minimization. In particular, we are interested in standard linear measurement problems of the form

$$\mathbf{y} = \mathbf{A}\mathbf{x} + \mathbf{w}, \quad (4)$$

where  $\mathbf{y} \in \mathbb{R}^m$  is the measurement,  $\mathbf{x} \in \mathbb{R}^n$  is the state to estimate,  $\mathbf{A} \in \mathbb{R}^{m \times n}$  is the matrix linking the state to the measurement, and  $\mathbf{w} \in \mathbb{R}^m$  is random Gaussian noise with covariance  $\Sigma$ . This formulation assumes that the error on the measurement can be modelled as a zero-mean, Gaussian random variable. Perturbations resulting from inclement weather or occlusions from other dynamic obstacles can contradict this assumption. Therefore, as is done in [9], we assume a measurement can be subject to both noise and a deterministic, possibly large, fault (corruption):

$$\mathbf{y} = \mathbf{A}\mathbf{x} + \mathbf{w} + \mathbf{Q}\mathbf{f}, \quad (5)$$

where  $\mathbf{f} \in \mathbb{R}^{n_f}$  are the faults, and  $\mathbf{Q} \in \mathbb{R}^{m \times n_f}$  is a sparse matrix of zeros and ones applying the faults to the associated measurements. As such, a part of the measurement is subject to a possibly large fault that can hinder the estimation.

In the context of linear estimation, the solution to a least-squares problem can be written as

$$\begin{aligned} \hat{\mathbf{x}} &= \arg \min_{\mathbf{x}} \sum_{i=1}^m \alpha_i \cdot (\mathbf{y}_i - \mathbf{A}_i \mathbf{x})^T \Sigma_i^{-1} (\mathbf{y}_i - \mathbf{A}_i \mathbf{x}) \\ &= \arg \min_{\mathbf{x}} (\mathbf{y} - \mathbf{A}\mathbf{x})^T \Sigma^{-1} (\mathbf{y} - \mathbf{A}\mathbf{x}), \end{aligned} \quad (6)$$

where  $\mathbf{y}_i$  is the  $i^{\text{th}}$  measurement with its associated covariance  $\Sigma_i$ , and  $\mathbf{x}$  is the pose to estimate. Note that each measurement is weighted by a factor  $\alpha_i$ , which is used to control the impact of each measurement on the estimate and is incorporated into the lifted matrix  $\Sigma$ .

Robust filters have the task of discriminating between inlier and outlier measurements. Among them, the trimmed distance filter is one of the most popular [2]. Given an initial guess  $\mathbf{x}_0$ , the trimmed distance filter removes any measurement that has a corresponding error that is larger than a fixed distance  $d$ :

$$\alpha_i = \begin{cases} 1 & \text{if } \|\mathbf{y}_i - \mathbf{A}_i \mathbf{x}_0\|_\infty \leq d, \\ 0 & \text{otherwise.} \end{cases} \quad (7)$$

As such, any fault trying to corrupt a system making use of a trimmed distance filter has to be small enough to be deemed an inlier. In the case of systems of the form defined in (6), the solution is given by

$$\hat{\mathbf{x}} = \mathbf{H}\mathbf{y}, \quad \text{with } \mathbf{H} = (\mathbf{A}^T \Sigma^{-1} \mathbf{A})^{-1} \mathbf{A}^T \Sigma^{-1}. \quad (8)$$

The corresponding state-estimation error can be computed as

$$\begin{aligned} \mathbf{e} &= \hat{\mathbf{x}} - \mathbf{x} \\ &= \mathbf{H}\mathbf{y} - \mathbf{x} \\ &= \mathbf{H}(\mathbf{A}\mathbf{x} + \mathbf{w} + \mathbf{Q}\mathbf{f}) - \mathbf{x} \\ &= \mathbf{H}(\mathbf{w} + \mathbf{Q}\mathbf{f}). \end{aligned} \quad (9)$$

The faults  $\mathbf{Q}\mathbf{f}$ , unlike the noise  $\mathbf{w}$ , are not zero-mean random variables, but are unknown, possibly large, deterministic quantities. As such, the faults generate a bias in the estimation that could be harmful. In the following, we provide a method to compute the worst error that can occur given corrupted measurements from a defined set.

### C. Safety Metric

Aiming at certifying a localization algorithm, we define a safety metric as the error on the pose being below a certain threshold:

$$|e_j| = |\mathbf{g}_j^T (\hat{\mathbf{x}} - \mathbf{x})| \leq r_j, \quad (10)$$

where  $\hat{\mathbf{x}}$  is the estimated state,  $\mathbf{x}$  is the ground truth,  $\mathbf{g}_j^T$  is a row matrix that extracts the  $j^{\text{th}}$  coordinate from the state, and  $r_j$  is the error-specific threshold. As such, an estimate is considered safe if each of its components has an error below a certain threshold  $r_j$ . Note that we choose to certify each component of the estimated state independently instead of looking at the  $L_2$  norm of the error. This is particularly useful in self-driving applications where, for instance, the lateral error is often more important than the longitudinal one. Using this definition, we seek to compute the probability that a pose estimate is safe:

$$p(|e_j| \leq r_j) \geq p_{\text{safe}}. \quad (11)$$

In other words, a given estimate is said to be certified if its probability to be in the safe zone of radius  $r_j$  is above  $p_{\text{safe}}$ . In the presence of faults, we are interested in the maximum number of faulted measurements that can happen at the same time before (11) becomes false. This quantity is defined as the *resilience* of the system.

## IV. CORRUPTED MEASUREMENTS

In this section, we provide a closed-form formula for the worst pose estimate given corrupted measurements from a defined set. This closed form is used to compute the probability that a pose estimate is hazardous, as defined in (11). Then, we define a metric to certify the resilience of ICP in different scenarios. Finally, we show how to link the faults back to a meaningful perturbation in the measured pointcloud.

### A. Worst Pose Estimate

This section proposes a closed-form formula to compute the probability of a pose estimate being hazardous, given corrupted measurements from a defined set. First, we define the constraint that the faults need to satisfy so that they are not trimmed by the outlier filter. As defined in (5), the measurement  $\mathbf{y}$  contains both a probabilistic zero-mean noise  $\mathbf{w}$  and deterministic faults from a defined set  $\mathbf{Q}\mathbf{f}$ . Faults that maximize the pose error will be such that they are considered inliers according to (7), but are otherwise maximally detrimental to the accuracy of the pose estimate. Using (5) and (7), assuming the initial guess is close to the ground truth, we have the following constraint on the faults:

$$\begin{aligned} \|\mathbf{y} - \mathbf{A}\mathbf{x}_0\|_\infty &\leq d \\ \Leftrightarrow \|\mathbf{w} + \mathbf{Q}\mathbf{f}\|_\infty &\leq d, \end{aligned} \quad (12)$$

meaning that all errors on the measurements are below the outlier detection threshold  $d$ . However, this constraint acts on the whole measurement vector and not only on the corrupted subset. As such, we reduce the constraint to only act on the subset of faulted measurements, as

$$\|\mathbf{Q}^T \mathbf{w} + \mathbf{f}\|_\infty \leq d, \quad (13)$$

where  $\mathbf{Q}^T \in \mathbb{R}^{n_f \times m}$  extracts the noise components of the faulted measurements from the noise vector  $\mathbf{w} \in \mathbb{R}^m$ . As such, the constraint (13) forces the faults to be small enough that the faulted measurements are still considered inliers. Using this constraint, we now seek to find the worst pose error that a defined set of faulted measurements could cause. Following (9) and (10), the maximum error that a set of faulted measurements can induce on the pose while being undetected by the outlier detector is defined by

$$\begin{aligned} \max_{\|\mathbf{Q}^T \mathbf{w} + \mathbf{f}\|_\infty \leq d} |e_j| &= \max_{\|\mathbf{Q}^T \mathbf{w} + \mathbf{f}\|_\infty \leq d} |\mathbf{g}_j^T \mathbf{H} (\mathbf{w} + \mathbf{Q}\mathbf{f})| \\ &= \max_{\|\mathbf{Q}^T \mathbf{w} + \mathbf{f}\|_\infty \leq d} |\mathbf{g}_j^T \mathbf{H} \bar{\mathbf{Q}} \mathbf{w} + \mathbf{g}_j^T \mathbf{H} \mathbf{Q} (\mathbf{Q}^T \mathbf{w} + \mathbf{f})|, \end{aligned} \quad (14)$$

where  $\bar{\mathbf{Q}} = \mathbf{I} - \mathbf{Q}\mathbf{Q}^T$ . In order to find a closed form, we recall that for all  $a \in \mathbb{R}$  and  $x \in [-m, m]$  we have

$$\max_{x \in [-m, m]} |a + x| = \max\{|a \pm m|\}. \quad (15)$$

As such, using (15), the worst error on the pose (14) can be rewritten as

$$\max_{\|\mathbf{Q}^T \mathbf{w} + \mathbf{f}\|_\infty \leq d} |e_j| = \max\{|\mathbf{g}_j^T \mathbf{H} \bar{\mathbf{Q}} \mathbf{w} \pm m|\}, \quad (16)$$

with

$$\begin{aligned} m &= \max_{\|\mathbf{Q}^T \mathbf{w} + \mathbf{f}\|_\infty \leq d} \mathbf{g}_j^T \mathbf{H} \mathbf{Q} (\mathbf{Q}^T \mathbf{w} + \mathbf{f}) \\ &= d \|\mathbf{g}_j^T \mathbf{H} \mathbf{Q}\|_\infty, \end{aligned} \quad (17)$$

where we used the fact that for any vectors  $\mathbf{a}, \mathbf{b}$ , we have

$$\max_{\|\mathbf{b}\|_\infty \leq 1} \mathbf{a}^T \mathbf{b} = \sum_k |a_k| = \|\mathbf{a}\|_\infty, \quad (18)$$

with  $\mathbf{a} = [a_1 \cdots a_N]^T$ . Plugging this back into (16), we finally find that the worst error on the pose is defined by

$$\begin{aligned} \max_{\|\mathbf{Q}^T \mathbf{w} + \mathbf{f}\|_\infty \leq d} |e_j| &= \max \left\{ \left| \mathbf{g}_j^T \mathbf{H} \bar{\mathbf{Q}} \mathbf{w} \pm d \|\mathbf{g}_j^T \mathbf{H} \mathbf{Q}\|_\infty \right| \right\} \\ &= \mathbf{g}_j^T \mathbf{H} \bar{\mathbf{Q}} \mathbf{w} + s \cdot d \|\mathbf{g}_j^T \mathbf{H} \mathbf{Q}\|_\infty, \end{aligned} \quad (19)$$

with  $s = \text{sgn}(\mathbf{g}_j^T \mathbf{H} \bar{\mathbf{Q}} \mathbf{w})$ . Therefore, for a given noise and set of corrupted measurements, the maximum error on the pose can be found in closed-form. Note, this equation yields the maximum error on the pose and not the fault vector that induces it.

In order to find the probability distribution of the worst error  $|e_j|$ , we use the notation  $v = \mathbf{g}_j^T \mathbf{H} \bar{\mathbf{Q}} \mathbf{w}$  and do the following manipulation:

$$\begin{aligned} p(|e_j| > r_j) &= p(e_j > r_j, v \geq 0) + p(e_j < -r_j, v < 0) \\ &= 2p(e_j > r_j, v \geq 0), \end{aligned} \quad (20)$$

where we group the  $v \geq 0$  and  $v < 0$  cases as  $v$  is a linear function of the noise  $\mathbf{w}$  and thus a zero-mean Gaussian random variable. Expanding the error  $|e_j|$ , we find

$$\begin{aligned} p(|e_j| > r_j) &= 2p\left(v + d \|\mathbf{g}_j^T \mathbf{H} \mathbf{Q}\|_\infty > r_j, v \geq 0\right) \\ &= 2p\left(v > \max\left\{r_j - d \|\mathbf{g}_j^T \mathbf{H} \mathbf{Q}\|_\infty, 0\right\}\right) \\ &= \min\{2(1 - \Phi_{\mu, \sigma}(r_j)), 1\}, \end{aligned} \quad (21)$$

where  $\Phi_{\mu, \sigma}(\cdot)$  is the standard cumulative distribution function of the normal distribution, with

$$\begin{aligned} \mu &= d \|\mathbf{g}_j^T \mathbf{H} \mathbf{Q}\|_\infty \\ \sigma^2 &= \mathbf{g}_j^T \mathbf{H} \bar{\mathbf{Q}} \Sigma_w (\mathbf{g}_j^T \mathbf{H} \bar{\mathbf{Q}})^T. \end{aligned} \quad (22)$$

In conclusion, this section provides a way to compute efficiently the probability of having a hazardous estimate of the pose given a malicious set of corrupted measurements, using (21). We show in the next section how to certify a map using this metric, before demonstrating how the faults on the point-to-plane measurements can be linked back to the measured lidar points.

### B. Map Certification

In the preceding section, we demonstrated the ability to determine efficiently the maximum localization error for a specific set of corrupted measurements. Nevertheless, due to the large number of points in a lidar scan, exhaustively testing every combination of corrupted points becomes impractical. To address this challenge, we propose to model the lidar field of view as a collection of angular sectors. All points within each sector are then either corrupted or unaltered. Although this assumption may appear restrictive, numerous events are inherently tied to a sector of corrupted points. For instance, cars parked on the side of the street will result in a coherent shift of the measured pointcloud compared to a map that was constructed without them present. Occlusions can also lead to a sector-wide pointcloud alteration, thus appearing as fully faulted sectors.

Using this modeling approach, we define the resilience  $R$  at a specific position on the map as the maximum proportion of the lidar scan that can be corrupted before the validity of the certificate stated in (11) is compromised.

### C. Fault Visualization

Although computing the explicit faults is not required for the safety assessment, it can be useful for visualization and evaluation purposes. As the faults are applied on the measurement equation defined in (5), the corruption is not linked to the measured points but rather the projected distance between the lidar points and the map. As such, in this section, we show how to recover a corruption on the pointcloud from a set of faults originally applied to the point-to-plane measurements. First, we recall that the vector that maximizes (18) is given by

$$\mathbf{b} = \text{sgn } \mathbf{a}, \quad (23)$$

where the sign function is extended to a vector, applying the sign function component-wise. As such, from (17) and (19), we can deduce that the fault vector  $\mathbf{f}$  that maximizes the error on the pose is

$$\mathbf{f} = s \cdot d \cdot \text{sgn} \left( \mathbf{g}_j^T \mathbf{H} \mathbf{Q} \right)^T - \mathbf{Q}^T \mathbf{w}. \quad (24)$$

Using (24), we are able to construct a fault vector on the point-to-plane measurements. However, this fault vector does not directly corrupt the measured points, which are 3D quantities, but rather the projected distances. To model point-wise corruption, we seek to find a perturbation  $\Delta \mathbf{p}_k$  for each measured point  $\mathbf{p}_k$  subject to corruption, with a perturbed point  $\mathbf{p}'_k$  defined as

$$\mathbf{p}'_k = \mathbf{p}_k + \Delta \mathbf{p}_k. \quad (25)$$

Rewriting (3) for one corrupted point, we have

$$\begin{aligned} \mathbf{n}_k^T (\mathbf{q}_k - \mathbf{p}'_k) &= -\mathbf{n}_k^T \mathbf{p}'_k \hat{\phi} + \mathbf{n}_k^T \mathbf{t} + \mathbf{w}_k \\ \Leftrightarrow \mathbf{n}_k^T (\mathbf{q}_k - \mathbf{p}_k) &= -\mathbf{n}_k^T \mathbf{p}_k \hat{\phi} + \mathbf{n}_k^T \mathbf{t} + \mathbf{w}_k \\ &\quad + \mathbf{n}_k^T \Delta \mathbf{p}_k - \mathbf{n}_k^T \Delta \mathbf{p}_k \hat{\phi}. \end{aligned} \quad (26)$$

Therefore, the fault on the point-to-plane measurement  $f_k$  is linked to the corrupted point by the relation

$$f_k = \mathbf{n}_k^T \Delta \mathbf{p}_k - \mathbf{n}_k^T \Delta \mathbf{p}_k \hat{\phi}, \quad (27)$$

from which we extract a viable solution

$$\Delta \mathbf{p}_k = f_k \mathbf{n}_k, \quad (28)$$

since  $\mathbf{n}_k^T \mathbf{n}_k \hat{\phi} = 0$ . Note that (27) possesses many solutions as we retrieve a 3D quantity from a 1D fault. From the perspective of our framework, all solutions are equally good, as all possible corruptions lead to the same corrupted point-to-plane measurements. However, (28) is particularly interesting as it is independent of the state variable  $\phi$ . As such, a fault on the point-to-plane measurement can be seen as a shift of the measured point along the associated map's normal. We use this fault modeling in Section V to show that the simplified ICP formulation used in the derivation of the framework is similar in behavior to a real ICP algorithm.

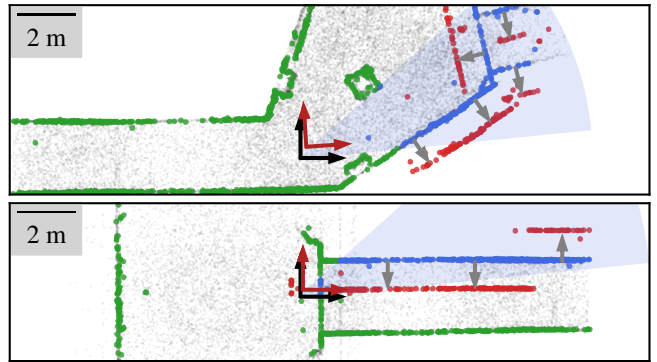


Fig. 2: Examples of faulted pointclouds from underground passages of the DARPA Subterranean challenge finals [24]. The faults try to corrupt the  $y$  component of the pose, with the corrupted pose estimated by ICP in red, and the ground truth pose in black. Black points correspond to the reference map. The lidar point cloud is illustrated in green, with a sector (shaded blue) being corrupted. The blue and red points correspond to the sector before and after corruption, with gray arrows showing the shift induced by the corruption. Points corresponding to the ceiling and floor are omitted for better visualization.

As examples, Figure 2 depicts two submaps of the DARPA Subterranean challenge finals [24], where a sector of the lidar scan is corrupted in a way to maximize the error in the  $y$  component of the pose. These maps depict underground environments with clear features that ICP is using to localize. The inlier threshold distance has been set to  $d = 1$  m. Using (24), we compute the worst faults on the  $y$  component for the given corrupted sector. The faults are then transformed back into a corruption on the pointcloud via (28). In the first example (top), the corrupted points shift and slightly rotate the pose estimate to achieve the worst  $y$  component estimate while evading an outlier detector. In the second example (bottom), the corruption takes a slightly more complex appearance. One might intuitively think that the worst pose estimate would come from shifting all the points in the same direction. However, our framework finds a more complex modification of the pointcloud that results in an even worse estimate. Indeed, a coherent shift of all points in a translation-only alignment problem would result in the worst estimate. However, as ICP has to estimate both the translation and the rotation components of the pose, shifting the whole wall in the same direction would make the ICP solution rotate instead of translate, as most of the pointcloud is left uncorrupted. Accordingly, the worst corruption modifies the pointcloud in such a way as to prevent rotation, resulting in a pure shift along the  $y$  axis.

## V. EXPERIMENTS

First, we evaluate the quality of our assumptions in the context of a real, iterative ICP. Then, we show the applicability of our method on real-world maps using the Boreas [25] and Montmorency Forest Wintertime [26] datasets.

### A. Quality of Approximations

As is done in HMI-based safety analysis (e.g., [8], [9]), our method reduces ICP to a linear, noniterative problem. This framework assumes a known data association between the map and the scan, which is impossible to have in practice. We show in this section that our framework yields an approximate upper-bound to a real iterative ICP algorithm, in which data association must be solved at each iteration. To do this, we sample 250 submaps from the `Boreas` dataset [25], in which we simulate a lidar scan from real lidar maps by subsampling the pointcloud. In this evaluation, 25% of the lidar scan is corrupted and perturbed using our framework, as this value is the highest resilience recorded in the experiments presented in Subsection V-B. Then, we feed this corrupted pointcloud to a vanilla ICP and compare the produced error with the theoretical one given by (19). Vanilla ICP is equipped with a trimmed distance filter, set to the same value  $d$  as in our framework.

Figure 3 depicts the signed difference between the theoretical errors predicted by our framework, and the real ICP errors generated from the corrupted scans, for different inlier threshold distances  $d$ . Overall, the difference in error exhibits a linear increase as the threshold distance  $d$  increases. It can be seen that our framework yields higher errors compared to those obtained by the ICP algorithm in more than 98% of cases. In cases where our framework predicts a lower error than the real ICP algorithm produces, the magnitude of error underestimation is on the order of centimeters and milliradians. As shown in the next section, our framework provides an estimate that is tight enough to pinpoint safe and hazardous regions within the maps. Future work will focus on providing a provable, tight upper bound.

For large inlier threshold distances, our framework overestimates the linear error up to 80 cm in rare cases. We theorize this discrepancy can be attributed to the fact that our framework assumes known data association and optimizes the perturbations accordingly. As the inlier threshold distance increases, the corrupted points deviate further from their true associated points in the map. Consequently, the likelihood of incorrect data associations also rises. In some instances where wrong data association occurs, it unexpectedly favours the ICP algorithm, as the perturbations applied were not optimized for that particular association. As a result, an overall reduction in the pose error may occur. On the other hand, the difference in rotational errors remains small. Owing to the nature of the environment, the considered scans contain discernible features far away from the robot. This makes it harder to corrupt the rotational component as compared to the translational one.

As such, assuming a known data association yields a reasonably conservative estimation on the error of ICP. This assumption is sensible as long as the environment features clear planes, as incorrectly associated points with the same plane will not affect the error terms. However, in the case of noisy normal estimates or unstructured objects, an incorrect data association can match points associated

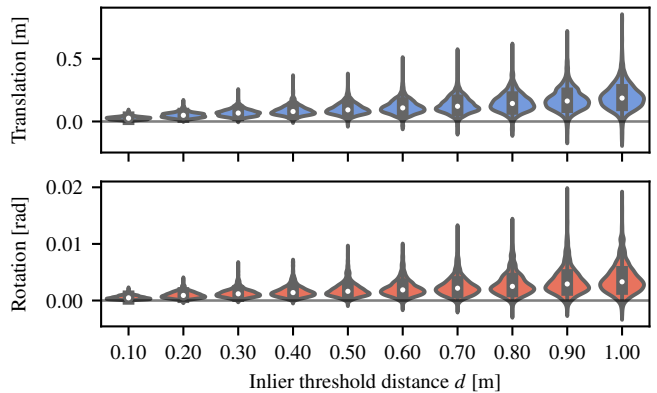


Fig. 3: Signed difference of ICP errors between our theoretical estimate and real ICP for different inlier threshold distances. The violins depict the overall distribution of the difference, whereas the white dots and black boxes stand for the median and quartiles. Our estimate typically yields larger errors compared to real ICP.

with different planes and thus returns a different error term. Such behavior is seen when our framework corrupts sectors containing bushes on the side of the road, or any other highly unstructured obstacles. These cases are responsible for the long tails of the distributions seen in Figure 3.

### B. Map Certification

To demonstrate the applicability of our framework for a given lidar map, we use the `Boreas` dataset [25] and certify the `Glensfield` trajectory. We sample poses along the trajectory and simulate a live scan by subsampling the map for each pose. The scan is then used to build the matrices in (3). For this experiment, we certify the map for both the longitudinal and lateral directions, ensuring that the probability of deviating from the true position by more than 20 cm is less than 1%. The outlier filter distance is set to  $d = 30$  cm and the noise  $w$  on the lidar measurements is equal to  $\sigma = 10$  cm. The lidar field of view is split into 30 sectors of approximately 0.1 rad. We compute the degree of resilience  $R$  for each pose and depict it in Figure 4. The vehicle starts in a parking lot before turning onto a main street (Figure 4.a). Then, the vehicle drives on smaller streets with better structural definition (Figure 4.b). Overall, the map is robust to an average corruption of around 15% of the pointcloud, with some exceptions. When turning onto the main road, the vehicle has to cross a large crossroad with almost no structure present in the pointcloud. As such, a small amount of faults is enough to push the estimate outside the safe bounds. While on the main street, few structures are close enough to help constrain ICP in the longitudinal direction, resulting in a drop of resilience to around 12%. In contrast, once the vehicle is on smaller streets with a lot of structural definition, ICP becomes resilient to a greater amount of corruption. Even if 20% of the scan is corrupted, there is still enough structure left untouched in the pointcloud to constrain ICP. Note that the two pointclouds depicted in Figure 4 correspond the same places pictured in Figure 1.

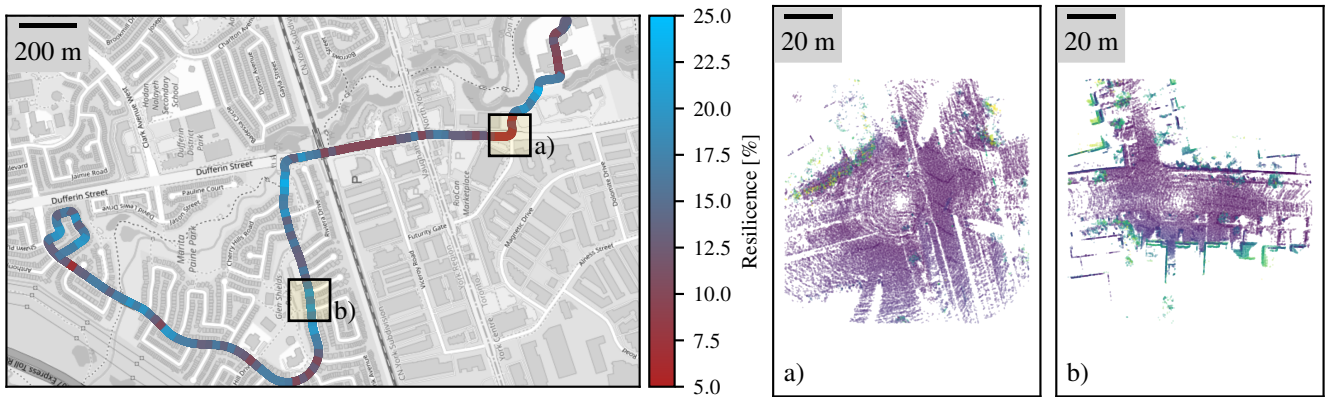


Fig. 4: Overall resilience of the Glenshield trajectory. The vehicle starts on the top right of the map, before driving on a large main road. It then leaves the road for smaller streets with better features. Left: overview of the trajectory, coloured by its resilience  $R$ . Right: Example of submaps with the colours representing the  $z$  component of the pointcloud for better visualization.

We additionally analyze a trajectory of the Montmorency Forest Wintertime dataset [26]. This dataset was taken in subarctic environments in Northern Quebec, Canada, and consists of both semi-structured surroundings and unstructured trails in wintertime. Figure 5 depicts the resulting resilience analysis on run A of the dataset. The robot starts at the bottom of the map inside a garage. It then drives next to a building before accessing a ski trail surrounded by tall pine trees. Overall, the resilience to faults is on the same order as in urban environments, as long as the robot remains close to structures. Once the robot reaches the ski trails and loses sight of the building, the resilience drops. Intuitively, the resilience of ICP is high when the robot is inside the garage, as there are good, clear structures against which to match. As the robot leaves the garage, the only structured obstacle is one wall of the building, as all other surrounding obstacles are snowbanks. Since ICP relies heavily on one locally concentrated obstacle, a fault in this part of the map leads to a large error in the pose estimate. As noted in [26], such faulted measurements were in fact observed during the recording of the dataset: a truck parked next to the wall resulted in the measurements being offset by a small value, yielding the same type of corruption as the one theorized in this paper. Harsh weather can also create similar effects, such as in the case of snow accumulating next to a building after a snowstorm overnight. As the robot drives toward the buildings on the top part of the figure, the resilience increases. The ICP algorithm can indeed rely on a diverse source of information to estimate the pose. As the robot continues driving, enough buildings are visible in the distance to maintain reasonable resilience even after the garage becomes out of view. The resilience goes down once again when the robot enters the ski trails, as it again only sees one part of a building. Once the robot drives along the trails, the resilience tends to drop down as it loses sight of the buildings.

In conclusion, our resilience analysis is able to highlight dangerous locations where a small amount of faults, coming

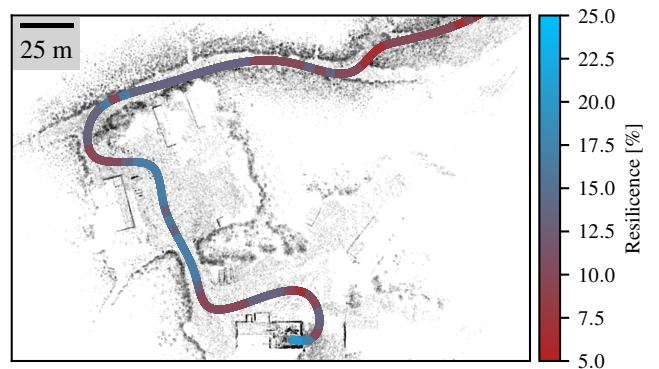


Fig. 5: Path A of the Montmorency Forest Wintertime dataset, coloured by its resilience to corruption  $R$ . The robot starts in a garage at the bottom of the map, proceeds to drive by several buildings, and finally enters a narrow ski trail surrounded by tall pine trees.

from occlusion, noise, or changes in the environment, could drastically hinder the localization process and lead the robot to hazardous behaviors. These situations can either come from a clear lack of good features in the environment, such as in the case of the large crossroad, or result from ICP relying too much on a single environmental feature. This second case can happen in semi-structured environment, as seen in the Montmorency Forest Wintertime dataset analysis.

## VI. CONCLUSION

In this paper, we present a novel way to analyze the resilience of the ICP algorithm. Resilience is defined as the maximum amount of faults that can be injected into the measurements before the localization estimate is dangerous for the robot. We model faults as the most severe modifications to the measurements that can go undetected by an outlier filter. Through this framework, we verify the quality of maps in both structured and unstructured environments, and demonstrate that environments lacking distinct, evenly distributed structures are more susceptible to inaccurate

estimates in the event of measurement corruption.

Future research will focus on addressing the assumptions made in this paper. We will account for the iterative nature of the ICP algorithm and explore a broader range of robust cost functions. Also, this paper assumes that the robot has a good initial guess. However, hazardous behavior can also occur during a sequence of bad ICP solutions, each driving the robot farther from the ground truth and feeding worse and worse initial guesses to the next iteration. As such, taking into consideration a possibly wrong initial guess will also help certify against a broader range of failures.

Finally, future work will involve expanding the framework to include other types of sensor failures, such as scenarios where a portion of the lidar becomes completely unavailable.

#### ACKNOWLEDGMENT

We would like to thank the Natural Sciences and Engineering Research Council of Canada (NSERC) and the Ontario Research Fund: Research Excellence (ORF-RE) program for supporting this work. We also thank the Northern Robotics Laboratory (Norlab) for their help with the datasets.

#### REFERENCES

- [1] C. Courcelle, D. Baril, F. Pomerleau, and J. Laconte, "On the importance of quantifying visibility for autonomous vehicles under extreme precipitation," *Towards Human-Vehicle Harmonization*, vol. 3, p. 239, Sep. 2022.
- [2] F. Pomerleau, F. Colas, and R. Siegwart, "A review of point cloud registration algorithms for mobile robotics," *Foundations and Trends in Robotics*, vol. 4, pp. 1–104, 1 2015.
- [3] M. Joerger, F.-C. Chan, and B. Pervan, "Solution separation versus residual-based RAIM," *NAVIGATION: Journal of the Institute of Navigation*, vol. 61, no. 4, pp. 273–291, 2014.
- [4] F. A. C. D. Oliveira, F. S. Torres, and A. Garcia-Ortiz, "Recent advances in sensor integrity monitoring methods - A review," *IEEE Sensors Journal*, vol. 22, pp. 10 256–10 279, 11 Jun. 2022.
- [5] P. Zhao, M. Joerger, X. Liang, B. Pervan, and Y. Liu, "A new method to bound the integrity risk for residual-based ARAIM," *IEEE Transactions on Aerospace and Electronic Systems*, vol. 57, pp. 1378–1385, 2 Apr. 2021.
- [6] J. A. Hage, P. Xu, P. Bonnifait, and J. Ibanez-Guzman, "Localization integrity for intelligent vehicles through fault detection and position error characterization," *IEEE Transactions on Intelligent Transportation Systems*, vol. 23, pp. 2978–2990, 4 Apr. 2022.
- [7] Q. Meng and L. T. Hsu, "Integrity monitoring for all-source navigation enhanced by Kalman filter-based solution separation," *IEEE Sensors Journal*, vol. 21, pp. 15 469–15 484, 14 Jul. 2021.
- [8] G. D. Arana, M. Joerger, and M. Spenko, "Efficient integrity monitoring for KF-based localization," in *2019 International Conference on Robotics and Automation (ICRA)*, IEEE, 2019, pp. 6374–6380.
- [9] O. A. Hafez, G. D. Arana, Y. Chen, M. Joerger, and M. Spenko, "On robot localization safety for fixed-lag smoothing: Quantifying the risk of misassociation," in *2020 IEEE/ION Position, Location and Navigation Symposium (PLANS)*, IEEE, 2020, pp. 306–317.
- [10] Y. Chen, O. A. Hafez, B. Pervan, and M. Spenko, "Landmark augmentation for mobile robot localization safety," *IEEE Robotics and Automation Letters*, vol. 6, no. 1, pp. 119–126, 2020.
- [11] T. Tuna, J. Nubert, Y. Nava, S. Khattak, and M. Hutter, "X-ICP: Localizability-aware lidar registration for robust localization in extreme environments," *arXiv preprint arXiv:2211.16335*, 2022.
- [12] J. Nubert, E. Walther, S. Khattak, and M. Hutter, "Learning-based localizability estimation for robust lidar localization," in *2022 IEEE/RSJ International Conference on Intelligent Robots and Systems (IROS)*, IEEE, 2022, pp. 17–24.
- [13] K. Ebadi, M. Palieri, S. Wood, C. Padgett, and A.-a. Aghamohammadi, "DARE-SLAM: Degeneracy-aware and resilient loop closing in perceptually-degraded environments," *Journal of Intelligent & Robotic Systems*, vol. 102, pp. 1–25, 2021.
- [14] Z. Zhang and D. Scaramuzza, "Beyond point clouds: Fisher information field for active visual localization," in *2019 International Conference on Robotics and Automation (ICRA)*, IEEE, 2019, pp. 5986–5992.
- [15] R. Aldera, D. De Martini, M. Gadd, and P. Newman, "What could go wrong? Introspective radar odometry in challenging environments," in *2019 IEEE Intelligent Transportation Systems Conference (ITSC)*, IEEE, 2019, pp. 2835–2842.
- [16] H. Carson, J. J. Ford, and M. Milford, "Predicting to improve: Integrity measures for assessing visual localization performance," *IEEE Robotics and Automation Letters*, vol. 7, pp. 9627–9634, 4 Oct. 2022.
- [17] L. Kong, Y. Liu, X. Li, R. Chen, W. Zhang, J. Ren, L. Pan, K. Chen, and Z. Liu, "Robo3D: Towards robust and reliable 3D perception against corruptions," *arXiv preprint arXiv:2303.17597*, 2023.
- [18] C. Xiang, C. R. Qi, and B. Li, "Generating 3D adversarial point clouds," in *2019 IEEE/CVF Conference on Computer Vision and Pattern Recognition*, 2019, pp. 9136–9144.
- [19] Y. Cao, C. Xiao, D. Yang, J. Fang, R. Yang, M. Liu, and B. Li, "Adversarial objects against lidar-based autonomous driving systems," *arXiv preprint arXiv:1907.05418*, 2019.
- [20] S. Yi, S. Worrall, and E. Nebot, "Metrics for the evaluation of localisation robustness," *IEEE Intelligent Vehicles Symposium (IV)*, pp. 1247–1253, Apr. 2019.
- [21] H. Delecki, M. Itkina, B. Lange, R. Senanayake, and M. J. Kochenderfer, "How do we fail? Stress testing perception in autonomous vehicles," in *2022 IEEE/RSJ International Conference on Intelligent Robots and Systems (IROS)*, IEEE, 2022, pp. 5139–5146.
- [22] K. Yoshida, M. Hojo, and T. Fujino, "Adversarial scan attack against scan matching algorithm for pose estimation in lidar-based slam," *IEICE Transactions on Fundamentals of Electronics, Communications and Computer Sciences*, vol. 105, no. 3, pp. 326–335, 2022.
- [23] T. Barfoot, *State Estimation for Robotics*. Cambridge, UK: Cambridge University Press, 2017.
- [24] K. Ebadi, L. Bernreiter, H. Biggie, G. Catt, Y. Chang, A. Chatterjee, C. E. Denniston, S.-P. Deschênes, K. Harlow, S. Khattak, *et al.*, "Present and future of SLAM in extreme underground environments," *arXiv preprint arXiv:2208.01787*, 2022.
- [25] K. Burnett, D. J. Yoon, Y. Wu, A. Z. Li, H. Zhang, S. Lu, J. Qian, W.-K. Tseng, A. Lambert, K. Y. Leung, *et al.*, "Boreas: A multi-season autonomous driving dataset," *The International Journal of Robotics Research*, vol. 42, no. 1-2, pp. 33–42, 2023.
- [26] D. Baril, S.-P. Deschênes, O. Gamache, M. Vaidis, D. LaRocque, J. Laconte, V. Kubelka, P. Giguère, and F. Pomerleau, "Kilometer-scale autonomous navigation in subarctic forests: Challenges and lessons learned," *Field Robotics*, vol. 2, pp. 1628–1660, 50 2022.